J. Fluid Mech. (1983), *vol.* 136, *pp.* 219–241
Printed in Great Britain

Pattern selection for finite-amplitude convection states in boxes of porous media

By PAUL H. STEEN
School of Chemical Engineering, Cornell University, Ithaca, New York 14853

(Received 31 January 1983 and in revised form 20 June 1983)

When a box of fluid-saturated porous material is heated from below, it is known that either a two- or three-dimensional convection pattern can occur depending on the initial configuration. By means of an analytic eigenfunction-expansion technique and a study of the phase-space dynamics of finite-amplitude disturbances we obtain (i) the regions within the space of initial conditions which lead to one or other of these competing states, and thereby (ii) the probability that a certain pattern will be realized, as well as (iii) the explicit form of the heat transferred by the patterns as it depends on aspect ratios. Cubic and nearly cubic boxes are considered, and the analysis applies for values of Rayleigh parameter from convection onset to 1.5 times critical. Our results correct several details appearing in the literature and explain observations made in previous numerical studies.

1. Introduction

A saturated porous medium heated from below will sustain a steady buoyancy-driven motion provided that a non-dimensional average vertical temperature gradient (a Rayleigh number) is moderate. For gradients that are too small, below a critical value, the saturating fluid is motionless and heat conduction occurs, while for too-large gradients time-dependent motions with varying degrees of complexity set in and heat convection dominates. We concentrate on the regime of *steady* convective motions and the resulting transport of heat, both of which are important in many thermomechanical and geophysical situations. See Combarnous & Bories (1975) for a description of these applications.

Convection in porous media in idealized situations has been studied numerically (e.g. Elder 1967; Straus & Schubert 1981) and in the laboratory (e.g. Schneider 1963; Elder 1967). These studies show that for a bounded region the particular convection pattern that occurs depends on the geometry of that region as well as the temperature gradient across it. Furthermore, Holst & Aziz (1972), Horne (1979) and Straus & Schubert (1979) have shown numerically for a cube with fixed parameters that two stable convection patterns, one two- and the other three-dimensional, can coexist. By trial they find that certain initial conditions lead to two-dimensional roll cells and others lead to a three-dimensional pattern. Straus & Schubert (1979) raise the question of whether it is 'possible to characterize from a probabilistic point of view sets of random initial conditions which lead to a particular dimensionality of convection.' They leave this question unanswered. Our study shows that such probabilities can be calculated at least over a range of Rayleigh numbers and that more importantly the physical mechanism by which disturbances lead to a certain pattern can be explained. This involves an examination of the dynamics within the phase-space of finite-amplitude disturbances to the conductive state. The specific results obtained

complement those of Straus & Schubert (1979, 1981) by filling in and correcting some of the details they present for lower Rayleigh numbers. The analytical structure we discover gives insight over the entire range of steady convection.

We consider convection in three-dimensional rectangular boxes filled with a saturated porous material and heated from below. The purpose is to discover the pattern structure of the multiple steady convection solutions, their domains of attraction in the space of initial disturbances, and show how those properties depend on the geometry of such boxes. We take the top and bottom of the box to be isothermal and the sides to be insulated. The fluid and solid properties are assumed constant. We present results for boxes whose dimensions lie near those of the cube so that our calculations may be compared with the numerical results of Straus & Schubert (1979), although the same methods apply for boxes of any dimension. For the cubic box convection first occurs at $R_c = 4\pi^2$ when a two-dimensional roll cell grows to a finite-amplitude pattern with R. We show that immediately above criticality it is the only stable pattern; the three-dimensional state found by Zebib & Kassoy (1978) is unstable, contrary to a statement of Straus & Schubert (1981) that it is the 'motion' for $4\pi^2 \leqslant R \leqslant 4.5\pi^2$. Another three-dimensional pattern comes into existence as a linear mode grows at $R = 4.5\pi^2$. However, we find it remains unstable from birth until $R = 4.87\pi^2$, when it gains stability and begins to compete with the two-dimensional pattern. This result corrects the lower bound to the Rayleigh-number range for stable three-dimensional convection given by Straus & Schubert (1981). Thereafter, and up to the point where modes we have not accounted for become important and our approximation breaks down, the two- and three-dimensional patterns remain the only stable states. An *a priori* estimate puts the breakdown point at about Rayleigh number 1.5 times critical. This is confirmed by calculations of the heat transferred across the box which agree well with those obtained numerically by Straus & Schubert (1979) up to that value.

Our analytical approach enables us to exhibit the boundaries which separate initial disturbances that evolve to either the three-dimensional or two-dimensional pattern. This permits a calculation of the probability that a particular pattern will occur, given an initial probability distribution of disturbances. We find for the cube and a Rayleigh number of 50 that there is a $21\,\% \pm 2\,\%$ chance that a disturbance of unit norm will lead to the three-dimensional pattern. Although conceptually simple, there are technical difficulties which have apparently prevented such calculations previously. One difficulty comes with the need to characterize all the accessible solutions (attractors). The structure of our problem allows us to show that there are no time-dependent attractors so that the only accessible solutions are the steady states. A second difficulty appears with the need to calculate 'separatrix surfaces' – those boundaries between the space-filling domains of attraction. To our knowledge this is the first example of such computations. When a fluid system has two or more stable steady states, experiments must be performed with a care that precludes disturbances which will take the system from one state to another. For the porous-media system such techniques which were previously part of the 'art' of the experimenter can now be made precise.

The geometric picture of the disturbance phase space for the nonlinear problem provides the insight as to why certain patterns are unstable and among the competing stable patterns why one is preferred over the others for a given initial condition. The following illustrates the complexity of the situation. At a Rayleigh number 1.4 times critical and for a box formed by stretching a cube in a horizontal direction, there are 29 distinct solutions (including the conduction state) of which there are three

qualitatively different stable patterns each with its own domain of attraction. The sequence that leads through increasing Rayleigh numbers to this situation begins below the critical value with the conduction state which is stable to all disturbances. When convection first occurs, there is a single stable pattern which grows to a small but finite amplitude, at which point a different finite-amplitude pattern stabilizes to a certain few disturbances. As Rayleigh number increases further, the new pattern becomes more popular and its domain of attraction grows. Finally a third finite-amplitude pattern gains stability and attracts its own set of disturbances in competition with the other two.

The analytical penetration into the nonlinear regime is possible owing to three circumstances. The first, independent of the problem, is the existence of an analytical Galerkin-like eigenfunction-expansion technique, originally proposed by Ekhaus (1965), and modified by Rosenblat (1979). As in standard procedures, the nonlinear solution is expanded as a sum of time-dependent amplitudes modifying the eigenfunctions associated with the linear operator, from which a system of ordinary differential equations determining the time dependence is deduced as a necessary condition. However, Rosenblat has shown it is possible to truncate to obtain bifurcation equations which apply for a range of the bifurcation parameter that includes several separated branch points (eigenvalues) of the linear problem. This differs from a procedure such as Stuart–Watson or Liapunov–Schmidt, where expansions are made about an isolated (although perhaps multiple) branch point. The approximation obtained via the modified technique is asymptotically valid for solutions of small amplitude and for a finite but limited range of bifurcation parameter. Our principal results come from an 11-mode truncation which is found to be a good approximation for $R < 1.5R_c \equiv R^*$ and amplitudes $O\{[(R^{*\frac{1}{2}} - R_c^{\frac{1}{2}})/R^*]^{\frac{1}{2}}\}$ (note our scaling in §2). Two effects can occur to limit the approximation. Modes not included in the interaction may become important and/or higher-order contributions by self-interactions of included modes may become significant. Rosenblat's technique has been used successfully in various other convection problems where there also occur bifurcations from multiple eigenvalues (Rosenblat, Davis & Homsy 1982; Rosenblat 1982). The second circumstance which forms a basis for our analysis is the simplicity of the eigenfunctions of the linear theory. They are products of sines and cosines, and hence the coefficients in the truncated system which are inner products of such terms can be obtained in closed form as functions of the box geometry. The third circumstance derives from the special structure of nonlinearity for the porous-medium problem. That structure allows the approximating system of nonlinear differential equations to be treated analytically and in a global sense, even though the powerful tools of phase-plane analysis are not available since the phase space for the system is of dimension higher than two.

We begin the study with a formulation of the problem, followed by a review of the existing linear theory and an outline of the method of finite-amplitude analysis. We then derive the equations that describe the interactions among three linearly unstable structures and which include the effects of geometry changes. Using this system, we first examine the cubic geometry and trace in detail the existence and stability of the multiple finite-amplitude convection patterns from $R = R_c$ to $R = 1.5R_c$ where the truncation ceases to be a good approximation. This analysis yields a complete determination of the pattern to which a particular disturbance will evolve and leads to an example calculation of the probability that a certain structure will occur. Then, the results for the cube, which include as a subcase those of Zebib & Kassoy (1978), are discussed and compared further with the numerical computations

of Straus & Schubert (1979). Finally, we trace the existence and stability sequence from $R = R_c$ for a rectangular box with dimensions near the cube but with non-square planform. Here we obtain the explicit form of the Nusselt number as a function of Rayleigh number and aspect ratios, appropriate within the limits of the approximation.

2. Formulation

Consider a rectangular box with horizontal aspect ratios h_1, h_2 relative to vertical height l and containing a porous material of permeability k and fixed porosity which is saturated with a Boussinesq fluid of viscosity ν and coefficient of thermal expansion α. The equations governing arbitrary disturbances (e.g. Homsy & Sherwood 1976) in the non-dimensional velocity, temperature and pressure fields $\boldsymbol{v}$, θ and p from the basic conduction state consisting of linear temperature profile extending from hot bottom plate (ΔT hotter) to cooler top plate are

$$\boldsymbol{\nabla}\cdot\boldsymbol{v} = 0, \tag{2.1a}$$

$$\mathbf{0} = -\boldsymbol{\nabla}p + R^{\frac{1}{2}}\theta\boldsymbol{k} - \boldsymbol{v}, \tag{2.1b}$$

$$\frac{\partial\theta}{\partial t} + R^{\frac{1}{2}}\boldsymbol{v}\cdot\boldsymbol{\nabla}\theta - R^{\frac{1}{2}}\boldsymbol{v}\cdot\boldsymbol{k} = \boldsymbol{\nabla}^2\theta. \tag{2.1c}$$

Here, since many porous materials of interest have low permeabilities, we have set the Prandtl number $(\nu/\kappa_m)\,l^2/k$ equal to infinity. The effective fluid–solid thermal diffusivity κ_m, which along with k enters the definition of the Rayleigh number $R \equiv g\alpha\Delta T k l/\kappa_m\nu$, make these numbers modified Rayleigh and Prandtl numbers. Here g is the magnitude of gravity, which acts vertically, antiparallel to the unit vector $\boldsymbol{k}$.

We have scaled (2.1) with characteristic length, velocity, temperature and time given by l, $R^{\frac{1}{2}}\kappa_m/l$, ΔT, and l^2H/κ_m respectively, where $H \equiv \rho_m C_{pm}/\rho_f C_{pf}$ is the ratio of heat capacity of the fluid–solid mixture to that of the fluid. Our velocity scale, which differs from that commonly used (e.g. Straus & Schubert 1979) by the factor $R^{\frac{1}{2}}$, leads to a convenient form of the linearized operator corresponding to (2.1).

The boundary conditions are isothermal top and bottom, insulated sidewalls, and no flow through the boundary of the box:

$$\theta = 0 \quad (z = 0, 1), \tag{2.1d}$$

$$\frac{\partial\theta}{\partial x} = 0 \quad (x = |\tfrac{1}{2}h_1|), \tag{2.1e}$$

$$\frac{\partial\theta}{\partial y} = 0 \quad (y = |\tfrac{1}{2}h_2|), \tag{2.1f}$$

$$\boldsymbol{v}\cdot\boldsymbol{n} = 0 \quad \text{on all boundaries.} \tag{2.1g}$$

Here we have used rectangular Cartesian coordinates with z increasing in a direction opposite to gravity, and the x- and y-axes parallel to the box sides in a right-handed system in which the centre of the box lies at $(0, 0, \frac{1}{2})$.

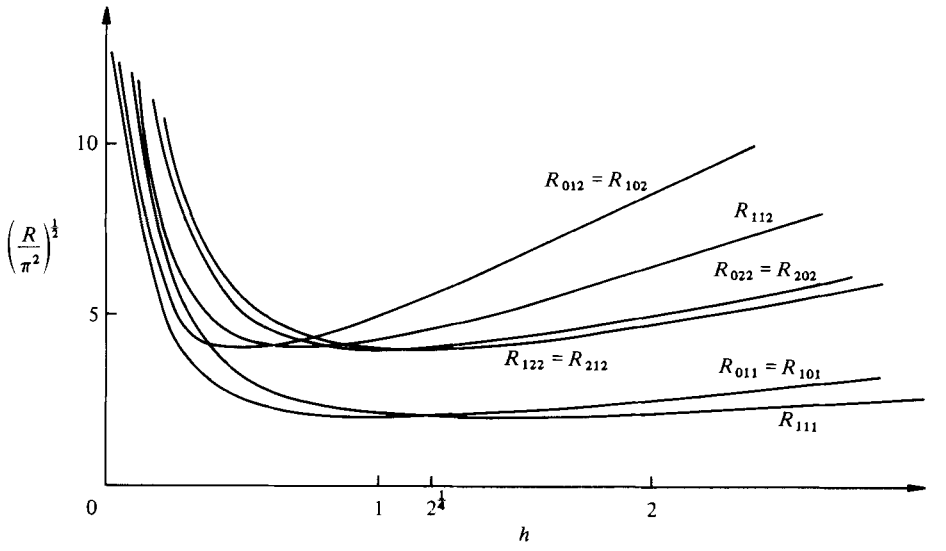

FIGURE 1. The Rayleigh numbers for neutral stability of several modes as a function of the dimension of the square planform ($h_1 = h_2 = h$). Four pairs of the neutral curves are coincident owing to the (x, y) symmetry.

3. Linear theory

The theory for the linearized version of (2.1) is due to Beck (1972). Separation of variables leads to a complete set of eigenfunctions $(\boldsymbol{v}_{lmn}, \theta_{lmn})$ with corresponding eigenvalues R_{lmn}, which characterize the non-oscillatory infinitesimal disturbances of the system. The disturbance structures are products of sines and cosines with wavenumbers (l, m, n) in the (x, y, z)-directions,

$$v_{1(lmn)} \equiv -n\pi L^{\frac{1}{2}}(L+M)^{-\frac{1}{2}} \sin l\hat{x} \cos m\hat{y} \cos n\pi z, \tag{3.1a}$$

$$v_{2(lmn)} \equiv -n\pi M^{\frac{1}{2}}(L+M)^{-\frac{1}{2}} \cos l\hat{x} \sin m\hat{y} \cos n\pi z, \tag{3.1b}$$

$$v_{3(lmn)} = (L+M)^{\frac{1}{2}}\theta_{(lmn)} \equiv \cos l\hat{x} \cos m\hat{y} \sin n\pi z, \tag{3.1c,d}$$

where $L \equiv (l\pi/h_1)^2$, $M \equiv (m\pi/h_2)^2$ and $\hat{x} \equiv (x+\frac{1}{2}h_1)\ \pi/h_1, \hat{y} \equiv (y+\frac{1}{2}h_2)\pi/h_2$.

The locus of points in the (R, h_1, h_2)-parameter space, for a fixed eigenfunction, for which infinitesimal disturbances neither grow nor decay is given by

$$R_{lmn} \equiv \left\{\left(\frac{l\pi}{h_1}\right)^2 + \left(\frac{m\pi}{h_2}\right)^2 + (n\pi)^2\right\}^2 \Big/ \left(\frac{l\pi}{h_1}\right)^2 + \left(\frac{m\pi}{h_2}\right)^2. \tag{3.2}$$

For each disturbance structure, labelled by its wavenumbers (l, m, n), this represents a neutral surface above the (h_1, h_2)-plane demarking the boundary between stability and instability for such disturbances. A section through some of those surfaces for boxes with square planform is shown in figure 1.

For most boxes there is a unique structure associated with the *most* unstable disturbance. However, as a map due to Beck (figure 2) of most unstable structure against box dimensions shows, there are segments of curves in the (h_1, h_2)-plane for which two structures are equally unstable and isolated points at which three and at most four different structures compete when the conduction solution loses stability.

We focus on the triple multiplicity at aspect ratios $(h_1, h_2) = (2^{\frac{1}{4}}, 2^{\frac{1}{4}})$, where an

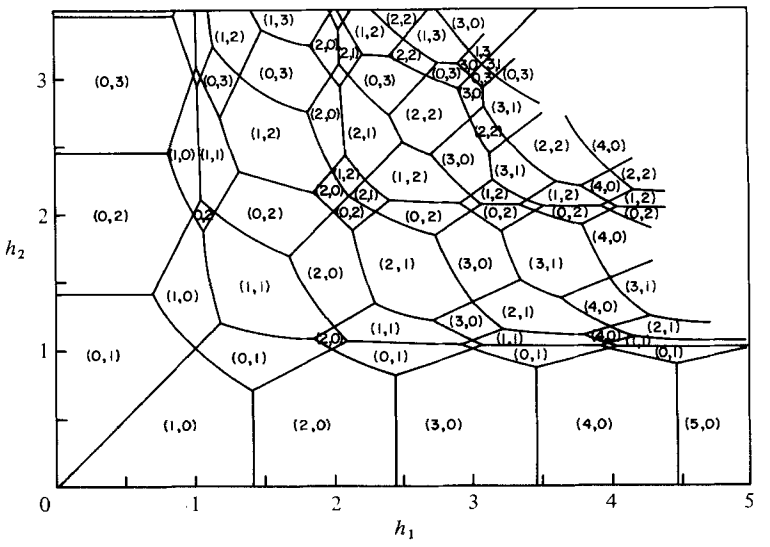

FIGURE 2. (After Beck 1972.) A map showing how the structure (x-, y-wavenumber) of the most-unstable disturbance depends on the aspect ratios h_1, h_2. The z-wavenumber for these disturbances is unity.

x-roll, y-roll and three-dimensional pattern compete, and treat the cube as a perturbation from that geometry. By a smooth deformation of that geometry to the cube the bifurcation structure at the triple multiplicity is also smoothly deformed to the structure we observe using Rosenblat's method. This guarantees that all of the bifurcations we observe at finite amplitude are present in the set of exact solutions to the partial differential equations – none have been introduced by the act of truncating. There is good reason to be careful concerning this point since cases where the truncation of an eigenfunction expansion have introduced spurious solutions are amply documented (Marcus 1981; Treve & Manley 1982; Rosenblat 1979).

4. Method of finite-amplitude analysis

Following Rosenblat (1982) we take the inner product of the nonlinear disturbance equations, considered as a vector equation for $\boldsymbol{x} \equiv (\boldsymbol{v}, \theta) \equiv [x_1, x_2, x_3, x_4]$, with the eigenfunctions of linear theory $\boldsymbol{x}_{lmn}$, to obtain a countable sequence of necessary conditions, one for each wavenumber triplet:

$$\left\langle \boldsymbol{x}_{lmn}, \boldsymbol{L}\frac{\partial \boldsymbol{x}}{\partial t}\right\rangle = (R_{\frac{1}{2}}^{\frac{1}{2}} - R_{lmn}^{\frac{1}{2}})\langle [0, 0, x_{4lmn}, x_{3lmn}], \boldsymbol{x}\rangle + \langle \boldsymbol{x}_{lmn}, \boldsymbol{N}(\boldsymbol{x}, \boldsymbol{x})\rangle \quad \text{for all } (l, m, n). \tag{4.1}$$

Here the $\langle\ ,\ \rangle$ indicates a Euclidean inner product of vectors followed by an integration over the volume of the box. The 4×4 matrix $\boldsymbol{L}$ has a single non-zero entry of unit value at the intersection of the fourth row and fourth column; only the time-derivative of the temperature appears on the left-hand side. $\boldsymbol{N}(\boldsymbol{x}, \boldsymbol{x})$ is a four-vector representing the convective nonlinearity; its only non-zero component appears in the fourth position and has the value

$$-R_{\frac{1}{2}}^{\frac{1}{2}}[x_1, x_2, x_3]\cdot\nabla x_4 \equiv -R_{\frac{1}{2}}^{\frac{1}{2}}\boldsymbol{v}\cdot\nabla\theta. \tag{4.2}$$

The solution is written as a finite sum of modes from linear theory each modified by a time-dependent amplitude. A mode is included if it meets one of two criteria:

(i) it grows according to linear theory at a given value of Rayleigh number – we call these primary modes;

(ii) it is produced by the quadratic nonlinear interaction (4.2) of two primary modes; this may be either by a mode interacting with itself or with another – these are called secondary modes.

For a good approximation to a fixed Rayleigh number, one expects that all the growing modes must be included. In this paper we shall judge validity by comparing our results with the numerical computations of Straus & Schubert.

The long-time dynamics of *any* disturbance sufficiently close to a sum of the unstable modes can be described in the finite-dimensional space of the amplitudes of these unstable modes. When there are two or more stable steady solutions, the probability that one will be realized given an arbitrary initial disturbance can be calculated on the basis of probabilities within the finite-dimensional subspace. This is demonstrated in §5.3.

5. Finite-amplitude convection near three competing linearly unstable structures

5.1. *Derivation of the amplitude equations*

As the temperature difference across a box with aspect ratios $(h_1, h_2) = (2^{\frac{1}{2}}, 2^{\frac{1}{2}})$ is increased, convection occurs at $R_c = 40.68$, where, by linear theory (figure 1), the x-roll, y-roll and a three-dimensional [111]-mode simultaneously go unstable. We seek an approximation to the full solution for an interval of Rayleigh numbers above critical for which these three are the *only* growing modes. Depending on the particular geometry (within a neighbourhood of $(h_1, h_2) = (2^{\frac{1}{2}}, 2^{\frac{1}{2}})$), the double x- or double y-roll is the next structure to go unstable and hence its omission from the set of primary modes gives an *a priori* limit in Rayleigh number to the validity of our approximation.

The three chosen primary modes interact through the nonlinearity to produce eight secondary modes as schematically illustrated in table 1. All secondary modes decay according to linear theory. However, if any of these interact, in turn, with the primaries to reproduce primaries, this spatial resonance can lead to finite-amplitude steady states. We assume a truncated solution

$$\boldsymbol{x}(t) = \sum_S a_{lmn}(t)\, \boldsymbol{x}_{lmn}, \tag{5.1a}$$

which consists of the primary and secondary modes whose indices are listed in the set

$$S \equiv \{(011), (101), (111), (002), (202), (022), (112), (212), (122), (012), (102)\}. \tag{5.1b}$$

Pairwise interaction of secondary with primary modes does reproduce primaries as indicated in table 1. It also yields others which we shall call tertiary modes. Using assumption (5.1) in (4.1), we calculate the projections on the primary and secondary eigenmodes ($(l, m, n) \in S$). This yields an eleven-dimensional first-order system of ordinary differential equations in the amplitudes a_{lmn}, $(l, m, n) \in S$. Here we have neglected the tertiary modes, since they are not coupled to the primaries and hence can be kept small by restricting to small primary amplitudes. Furthermore, we may reduce from an 11- to a 3-dimensional system by putting the rates of changes of the

				Primary	Secondary		Secondary				
	Primary			Secondary			Primary				
							Tertiary				
	Secondary			Primary			Quarternary				
				Tertiary							
s... / *r*	101	011	111	002	202	022	112	012	102	212	122
101	002	112	012	101	101	121	011	111	001	111	221
			212	103	301	123	013	113	201	113	021
					303		211		003	311	223
					103		213		203	313	023
011		002	102	011	211	011	101	001	111	201	111
			122	013	213	013	103	003	113	203	113
						031	121	021		221	131
						033	123	023		223	133
111			002	111	111	111	001/221	101	011	101/301	011/031
			202	113	113	113	003/223	103	013	103/321	013/033
			022		131	131	021/201	121	211	121/303	211/231
					133	133	023/203	123	213	123/323	213/233

TABLE 1. The modes produced by the symmetric part of the nonlinear interaction $N(r,s)+N(s,r)$ of modes r and s for the 11-mode truncation. The primary modes mix to yield secondary modes, which can then interact with the primaries to reproduce primaries (underlined) as well as tertiary modes. The quarternary modes due to fourth-order interactions are not shown.

eight secondary modes to zero, and then eliminating those modes from the other three equations.

To illustrate this procedure we specialize to the simplest physical subcase of our 11-mode truncation. For aspect ratios $(h_1, h_2) = (2^{\frac{1}{2}}, 2^{\frac{1}{2}}-\epsilon)$, ϵ a small positive number, the y-roll goes unstable first and very close to onset the solution can be represented by the growing y-roll $\boldsymbol{x}_{011}$ and a single secondary mode, the motionless temperature field $\boldsymbol{x}_{002}$:

$$\boldsymbol{x} \equiv a(t)\,\boldsymbol{x}_{011} + b(t)\,\boldsymbol{x}_{002}.$$

Substitution in (4.1) yields the system of amplitude equations

$$\frac{\mathrm{d}a}{\mathrm{d}t} = (R^{\frac{1}{2}} - R_c^{\frac{1}{2}})\frac{2\pi}{h_2}a + R^{\frac{1}{2}}\frac{\pi^2}{h_2}ab, \tag{5.2a}$$

$$\frac{\mathrm{d}b}{\mathrm{d}t} = -8\pi^2 b - R^{\frac{1}{2}}\frac{\pi^2}{h_2}a^2, \tag{5.2b}$$

which neglects the higher-order mode [013] produced by the mixing of the primary [011] and secondary [002] modes. This may restrict the analysis to small amplitudes of the primary mode. Although the quantity $R^{\frac{1}{2}} - R_{002}^{\frac{1}{2}}$ is infinite, the product

$$(R^{\frac{1}{2}} - R_{002}^{\frac{1}{2}})\,\langle [0, 0, x_{4002}, x_{3002}], \boldsymbol{x}_{002}\rangle,$$

is finite and takes the value $-8\pi^2$, as can be seen by a simple argument which views the motionless [002]-state as a limiting case of long-wavelength motion.

Close to the onset of convection, the secondary mode will equilibrate much more rapidly than the primary mode and hence we may set its time derivative in (5.2b)

to zero. Solving that equation for the secondary mode, and substituting in (5.2*a*), yields the Landau-type equation

$$\frac{\mathrm{d}a}{\mathrm{d}t} = (R^{\frac{1}{2}} - R_c^{\frac{1}{2}})\frac{2\pi}{h_2}a - \frac{R\pi^2}{8h_2^2}a^3. \tag{5.3}$$

This simplification preserves both the structure and stability of the steady solutions, as verified by comparing a phase-plane analysis of system (5.2) with the solutions of (5.3).

For the 11-mode truncation the same properties are preserved provided the amplitudes of the primary modes are sufficiently small (finite-dimensional Invariant Manifold Theorem – e.g. Hartman 1964, theorem 6.2, p. 243). The reduced three-dimensional system can be put in final form by the change of variables

$$x \equiv a_{101}^2, \quad y \equiv a_{011}^2, \quad z \equiv a_{111}^2 \tag{5.5a, b, c}$$

to yield

$$(2\pi)^{-1}\frac{\mathrm{d}x}{\mathrm{d}t} = x\left\{\frac{2(R^{\frac{1}{2}} - R_{101}^{\frac{1}{2}})}{h_1} - R[F(h_1)\,x + B(h_1, h_2)\,y + C(h_1, h_2)\,z]\right\}, \tag{5.5a}$$

$$(2\pi)^{-1}\frac{\mathrm{d}y}{\mathrm{d}t} = y\left\{\frac{2(R^{\frac{1}{2}} - R_{011}^{\frac{1}{2}})}{h_2} - R[B(h_2, h_1)\,x + F(h_2)\,y + C(h_2, h_1)\,z]\right\}, \tag{5.5b}$$

$$(2\pi)^{-1}\frac{\mathrm{d}z}{\mathrm{d}t} = z\{(R^{\frac{1}{2}} - R_{111}^{\frac{1}{2}})\,A - R[D(h_1, h_2)\,x + D(h_2, h_1)\,y + E(h_1, h_2)\,z]\}, \tag{5.5c}$$

where

$$A^2 \equiv \frac{1}{r^2} + \frac{1}{s^2}, \tag{5.6a}$$

$$B(r, s) \equiv \frac{\pi}{8}\left\{\frac{1}{rs} - \frac{1}{2}\left[\left(\frac{R}{\pi^2}\right)^{\frac{1}{2}} - \left(A + \frac{4}{A}\right)\right]^{-1}\left(\frac{1}{A}\left(\frac{1}{s^2} - \frac{1}{r^2}\right) + \frac{1}{s}\right)\left(\frac{1}{r} + \frac{1}{s}\right)\frac{1}{A}\right\}, \tag{5.6b}$$

$$\begin{aligned} C(r, s) \equiv \frac{\pi}{8}\Bigg\{&\frac{A}{2r} - \frac{1}{8}\left[\left(\frac{R}{\pi^2}\right)^{\frac{1}{2}} - \left(G + \frac{4}{G}\right)\right]^{-1}\frac{1}{[GAs]^4}\left(\frac{1}{A} + \frac{1}{G}\right) \\ &- \frac{s}{4}\left[\left(\frac{R}{\pi^2}\right)^{\frac{1}{2}} - \left(\frac{1}{s} + 4s\right)\right]^{-1}\left(\frac{1}{s} + A + \frac{1}{r^2 A}\right)\left(\frac{2}{r} + A + \frac{1}{r^2 A}\right)\Bigg\}, \end{aligned} \tag{5.6c}$$

$$\begin{aligned} D(r, s) \equiv \frac{\pi}{16}\Bigg\{&\frac{A}{r} - \frac{s}{2}\left(\frac{2}{r} - \frac{1}{s}\right)\left[\left(\frac{R}{\pi^2}\right)^{\frac{1}{2}} - \left(\frac{1}{s} + 4s\right)\right]^{-1}\left(\frac{2}{r} + A + \frac{1}{r^2 A}\right) \\ &+ \frac{1}{4}\left[\left(\frac{R}{\pi^2}\right)^{\frac{1}{2}} - \left(G + \frac{4}{G}\right)\right]^{-1}\frac{1}{G^2 s^4 A}\Bigg\}, \end{aligned} \tag{5.6d}$$

$$E(r, s) \equiv \frac{\pi}{16}\left\{\frac{A^2}{2} - \frac{1}{4A^2}[H(r, s) + H(s, r)]\right\}, \tag{5.6e}$$

$$F(r) \equiv \frac{\pi}{8}\left(\frac{1}{r^2}\right), \quad G^2(r, s) \equiv \frac{4}{r^2} + \frac{1}{s^2}, \tag{5.6f, g}$$

$$H(r, s) \equiv \frac{r}{s^4}\left\{\left(\frac{R}{\pi^2}\right)^{\frac{1}{2}} - 2\left[\frac{1}{r} + r\right]\right\}^{-1}. \tag{5.6h}$$

The coefficient F which arises from the resonant interaction of the motionless temperature field ([002]-mode) with the x- and y-roll structures is always positive. The self-interaction of the x-roll produces a stabilizing contribution to the motionless temperature field which in turn stabilizes the growth of the x-roll. Balanced by the linear growth of the x-roll, a steady finite-amplitude roll-pattern becomes possible.

Such an interplay produced the solution of (5.3). However, the influence on the growth of the x-roll by the interaction with the other modes complicates the situation here.

The growth-limiting effect (due to three-step interactions) which the x-roll (and y-roll, by symmetry) exerts upon itself is due to a single resonant interaction path which leads through the motionless temperature field ([002]-mode). On the other hand, each of the coefficients B, C, D and E has, besides the contribution through the motionless temperature field represented by the first term within the curly brackets, other contributions due to alternate interaction paths. Each of these other terms in each of the coefficients has a factor in the denominator which depends on R and is of the form

$$\pi[R_{\frac{1}{2}}^{\frac{1}{2}} - R_{lmn}^{\frac{1}{2}}].$$

These represent the distance of the parameter $R_{\frac{1}{2}}^{\frac{1}{2}}$ from the point of linear instability of the mediating mode. For example, in the coefficient B the [112]-mode mediates, while in coefficient $C(h_1, h_2)$ both the [212]- and [102]-modes are intermediaries. Since all the intermediaries are secondary modes, they are linearly stable for $R < 60$ (figure 1), the range of good approximation, and therefore each of these factors is negative. In coefficients C and E they multiply negative terms, and hence yield a positive contribution to the coefficient and add to its growth-limiting effect. However, in coefficients B and D the negative factors multiply terms which can have either sign depending on the aspect ratios. Nevertheless, computations show that coefficients B and D are growth-limiting for all $0.5 \leqslant h_1, h_2 < 1.5$ and for $R < 60$, suggesting that when growth-enhancing effects appear they are overcome by the growth-limiting effects of the first term in these coefficients. In summary, all the interactions tend to stabilize the growth of the primary modes in the regime where our approximation applies. This leads to the question: which of these apparent solutions is preferred and why? Sections 5.2 and 5.5 examine the solutions of system (5.5) and discuss this question in two different cases.

5.2. *The cubic box*

For comparison with and extension of previous results, we first study system (5.5) at the cubic geometry $(h_1, h_2) = (1, 1)$ where $R_c \equiv R_{101} = R_{011} = 4\pi^2 < R_{111} = 4.5\pi^2$. As first pointed out by Bauer, Keller & Reiss (1975), such 'splitting' of multiple eigenvalues may lead to secondary bifurcations. This has been illustrated for various convection problems by Rosenblat *et al.* (1982) and Rosenblat (1982). The 'splitting' parameter Δ is defined to be

$$\Delta \equiv R_{111}^{\frac{1}{2}} - R_c^{\frac{1}{2}} = 0.38,$$

and we call the distance from convection onset

$$\lambda \equiv R^{\frac{1}{2}} - R_c^{\frac{1}{2}}.$$

This brings (5.5) into the form

$$(2\pi)^{-1}\frac{dx}{dt} = x\{2\lambda - R[Fx + By + Cz]\}, \tag{5.7a}$$

$$(2\pi)^{-1}\frac{dy}{dt} = y\{2\lambda - R[Bx + Fy + Cz]\}, \tag{5.7b}$$

$$(2\pi)^{-1}\frac{dz}{dt} = z\{\sqrt{2}\,(\lambda - \Delta) - R[Dx + Dy + Ez]\}, \tag{5.7c}$$

where the coefficients are evaluated at $(h_1, h_2) = (1, 1)$ and depend only on R. The phase space for solutions of system (5.7) is the positive octant of (x, y, z)-space. Each

quantity in brackets on the right-hand side vanishes on a plane in three-space, and when such planes intersect the positive octant they partition it into regions in which the triplet of derivatives maintains the same signs. The relative positions of these planes in space varies with λ and determines the number, structure and stability of the convection patterns.

The partitioning of the phase space into regions bounded by planes is the property of system (5.7) which makes the global analysis possible. And such a structure is a more general property of the convection system than may be evident from our analysis so far. Indeed, as long as the modes in the truncation are selected by the criteria outlined in §4, and only second-order interactions are considered, any truncated system given through (4.1) can be reduced to a system partitioned by hyperplanes. To see this consider the nonlinear interaction between any ($\boldsymbol{v}$, θ) satisfying boundary conditions (2.1*d–g*),

$$\langle \theta \boldsymbol{v} \cdot \boldsymbol{\nabla} \theta \rangle = 0.$$

By choosing $\theta \equiv \theta_1 + \theta_2$, $\boldsymbol{v} \equiv \boldsymbol{v}_3$, one obtains

$$\langle \theta_1 \boldsymbol{v}_3 \cdot \boldsymbol{\nabla} \theta_2 \rangle = -\langle \theta_2 \boldsymbol{v}_3 \cdot \boldsymbol{\nabla} \theta_1 \rangle$$

for any modes θ_1, θ_2, $\boldsymbol{v}_3$. This means that (i) the mixing of a mode with itself cannot directly produce a contribution to its own growth, and (ii) if the nonlinear combination $ca_3 a_2$ appears in the evolution equation for a_1 then there must appear a corresponding term $-ca_3 a_1$ in the a_2 evolution equation. Writing down the linear and nonlinear contributions shows that a first-order quadratic system can be reduced to a first-order cubic system in only the growing modes. Furthermore, a change of variables analogous to (5.4) is possible provided that only one secondary mode is produced by each mixed interaction of primaries, and will deliver a system with the structure described above. We return to an analysis of system (5.7).

Below critical, $\lambda < 0$, all three modes decrease in amplitude throughout the octant and the conduction state, the unique solution, is stable. At convection onset, $\lambda = 0$, the planes where the curly brackets in (5.7*a*, *b*) vanish, which we shall call planes I and II respectively intersect the octant at the origin. On the other hand, plane III, named analogously, has no points in common with the octant, so that z is decreasing everywhere there. As λ increases, planes I and II cut the octant and intersect each other in a line as shown in figure 3(*a*). This qualitative picture holds for $0 < \lambda \leqslant 0.38$ ($4\pi^2 < R \leqslant 4.5\pi^2$).

Over this Rayleigh-number interval there are three steady solutions of system (5.7) in addition to the conduction solution. They are of two types: the *pure modes* where only one amplitude does not vanish, and a *mixed 2-mode* where two amplitudes are non-zero. Here, the pure modes are x-roll and y-roll convection patterns, marked by circles on the respective axes in figure 3. The magnitudes are given by $(2/RF)\,\lambda$. The mixed 2-mode is a prescribed linear combination of x- and y-roll with equal parts of both by symmetry, and with magnitudes $\lambda(2/R)\,(F\text{–}B)/(\det)$, where

$$\det \equiv F^2 - B^2. \tag{5.8}$$

The classification of steady convection solutions is completed with a third type, the *mixed 3-mode*, for which all three amplitudes are non-zero. Such a solution comes into existence at higher Rayleigh number, as we shall see.

For each pure-mode solution, say $x = c$, there correspond two steady convection solutions (definition (5.4)),

$$a_{101} = \pm c^{\frac{1}{2}}.$$

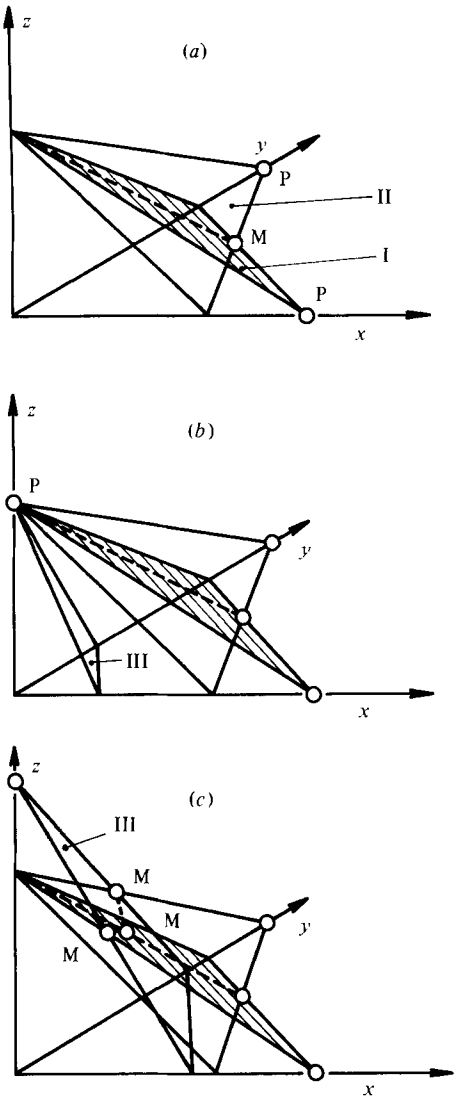

FIGURE 3. Phase-space pictures for the cubic box, giving the steady convection solutions (circles) as determined by the intersections of planes I, II, and III, which move relative to one another as R/R_c increases from 1.125 (*a*) through 1.218 (*b*) to 1.5 (*c*). The pure modes are denoted by P and mixed mode by M; the distance of planes I and II from the origin has been normalized.

Each differs from the other by a reversal in direction of flow. With our assumption of constant physical properties, neither of these two solutions is preferred over the other. For a mixed 2-mode solution $(x, y) = (a, b)$, there correspond four convection solutions,

$$(a_{101}, a_{011}) = (a^{\frac{1}{2}}, b^{\frac{1}{2}}), \quad (-a^{\frac{1}{2}}, -b^{\frac{1}{2}}), \quad (a^{\frac{1}{2}}, -b^{\frac{1}{2}}), \quad (-a^{\frac{1}{2}}, b^{\frac{1}{2}}).$$

In a similar way, the mixed 3-mode in (x, y, z)-space generates eight convection solutions, each differing from another by a sign change of one of its components.

The stability of the solutions we are considering ($0 < \lambda \leqslant 0.38$) can be read off the geometrical phase-space picture. Since $z(t)$ decreases everywhere in the octant above the $z = 0$ plane, all trajectories approach the plane. It is sufficient to consider the stability of the solutions in that plane (an invariant set). One can show by phase-plane

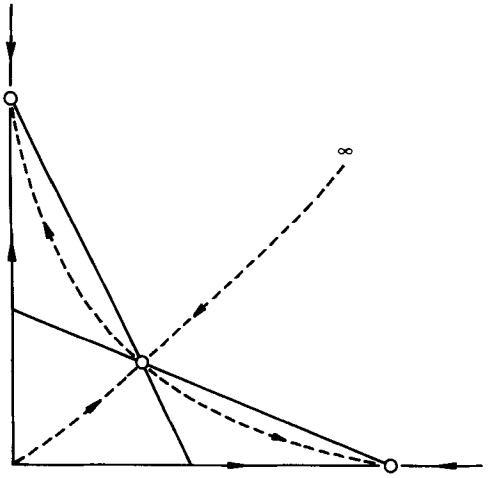

FIGURE 4. The phase plane (quadrant) with the dynamics typical when a mixed mode (circle in interior) is produced by the interaction of two pure modes (circles on axes). The mixed solution is a saddle with separatrix curves (dashed), whose stabilities are given by the arrows. The origin, the conduction solution, is unstable.

methods that the stability of the mixed 2-mode and the pure modes depends on the determinant (5.8). The mixed mode is unstable (stable) and the pure modes stable (unstable) for det $\leqslant 0$ (> 0). Geometrically, this can be phrased in terms of the angle relative to the origin formed by the lines whose intersection represents the mixed mode (figure 4). Indeed, if that angle is re-entrant, the mixed mode (pure modes) is (are) unstable (stable). In the case under consideration, $B(1,1)/F(1,1) > 1$, and the linear combination of orthogonal x- and y-roll cells is unstable. This is the pattern which Zebib & Kassoy (1978) first discovered.

For $\lambda > 0.38$ the 111-mode is unstable by linear theory and plane III cuts the positive octant; its intersection with the z-axis gives a finite amplitude 111-convection solution. Figure 3(b), drawn at the point at which plane III just intersects plane I and II ($\lambda = 0.66$, $R = 4.87\pi^2$), gives the qualitative picture for $0.38 < \lambda \leqslant 0.66$. Up to $\lambda = 0.66$, the 111-pure mode solution is in a region where $\mathrm{d}x/\mathrm{d}t, \mathrm{d}y/\mathrm{d}t \geqslant 0$, and hence is unstable. Over this interval the other three solutions maintain the stability they possessed for $0 < \lambda \leqslant 0.38$.

At $\lambda = 0.66$, three new solutions are born, including a mixed 3-mode. The latter is represented by the intersection of planes I, II and III in figure 3(c) with the magnitudes of its components given by the solution of the corresponding linear system. The other two are an (x, z) and (y, z) mixed 2-mode located in the $y = 0$ and $x = 0$ invariant quarterplanes respectively. The stability of these latter solutions is determined by a combination of the stability in the plane and that normal to the plane. The geometric criterion presented in the discussion of the (x, y) mixed 2-mode applies for the in-plane stability. Accordingly the mixed mode is unstable *in the plane*. Of course this is sufficient for instability in 3-space.

To summarize, for $\lambda > 0.66$ there are three mixed 2-modes, each lying in a face of the positive octant. Each of the invariant quarterplanes containing a mixed 2-mode has qualitatively the same dynamics, shown in figure 4. The stationary solution is a saddle point with two stable trajectories, one each from the origin and from infinity. Particle paths along the two unstable trajectories lead to the two adjacent pure modes. This gives four separatrixes which partition the quarterplane, and the union

	Increasing λ ⟶
Pure mode,	
x	(0) ⟶
y	(0) ⟶
z	(0.38) ⟶
Mixed 2-mode	
(x, y)	(0) ⟶
(x, z)	(0.66) ⟶
(y, z)	(0.66) ⟶
Mixed 3-mode	
(x, y, z)	(0.66) ⟶

TABLE 2. This birth chart for the cubic box gives the distance λ from convection onset at which a convection solution is born

of the two stable trajectories divides the space into two domains of attraction, one for each pure mode. Any initial condition on one side of the dividing line evolves to the same pure-mode convection state.

Before considering the stability of the newborn mixed 3-mode, we examine the pure modes which persist from lower Rayleigh numbers. Figure 3(*c*) shows that in a neighbourhood of the x-roll, say, both $y(t)$ and $z(t)$ are monotone decreasing except on the x-axis. There the roll is stable with respect to one-dimensional disturbances. It follows that the x-roll is linearly stable in the three-dimensional phase space. An analogous argument applies to the other pure modes, with the result that they are also locally stable in phase space.

The mixed 3-mode convection solution, a linear combination of the x-roll, y-roll and the three-dimensional [111]-mode, is linearly unstable as a straightforward calculation shows. The $x = y$ quarterplane which passes through the mixed 3-mode is an invariant set of points by symmetry. In that plane, the 3-mode is a saddle with stable trajectories coming from the origin and infinity and unstable trajectories leading to the [111] pure mode and the (x, y) 2-mode (figure 4).

The phase-space picture does not change qualitatively for $0.66 < \lambda$. However, our 11-mode truncation with three-step interactions fails to capture higher-order contributions which become significant for $\lambda \approx 1.55$ so this picture cannot be expected to be accurate beyond there.

The existence and stability of solutions from convection onset is summarized in a birth chart (table 2). As the x- and y-roll go unstable by linear theory, finite-amplitude locally stable x- and y-roll convection patterns are born, and an arbitrary small-norm disturbance will be attracted to one or the other depending on where its initial conditions falls in the phase space. By symmetry the domains of attraction occupy equal volumes. A linear combination of the orthogonal rolls also exists, but is unstable. At $R = 4.5\pi^2$, a three-dimensional finite-amplitude mode is born but remains unstable to the x- and y-roll patterns until $R = 4.87\pi^2$, where it becomes locally stable. As R is increased further, its domain of attraction expands. As the stability character of the [111]-mode changes, there occurs simultaneously the birth of the three new solutions, all of which are unstable. Two are linear combinations (with prescribed proportions) of two pure modes, called mixed 2-modes, and one is a linear combination of three pure modes, a mixed 3-mode. The symmetries of transformation (5.4) give for these Rayleigh numbers a total of 26 distinct convection solutions, of

which 7 have different modal compositions. Of these, only the x-roll, y-roll and [111]-mode are stable. We shall discuss the heat-transport properties of these solutions in §5.4.

5.3. *The probability of pattern selection: an example*

In any numerical or laboratory experiment disturbances to the system may in general include contributions from any of the infinite number of modes. Theory dictates that close to convection onset and for disturbances of small amplitude only three of these modes are involved in the equilibrium states. Furthermore, the phase-space pictures of §5.2 show that the selection of a particular pattern depends only on the relative contributions of the three modes to the disturbance amplitude. However, in experiments and with some numerical techniques, it is often difficult and sometimes impossible to control the character of disturbances. More usual is a situation in which large disturbances can be excluded. Hence we consider the probability that a pattern will be selected given disturbances with norms less than a certain value. Note that since a projection of a disturbance is always smaller than the disturbance, it is meaningful to consider probabilities within the three-dimensional subspace of projections.

To each attractor belongs a domain of attraction, and the volume fraction of the phase space occupied by a domain determines the probability that a particular pattern will be selected. We have found the steady-state attractors in §5.2 and now must show there are no time-dependent attractors before mapping out the boundaries between the domains of attraction.

First consider the $x = y$ invariant quarterplane which passes through the mixed 3-mode. It has the same qualitative structure as the other three invariant planes (figure 4). In particular, a phase-plane analysis demonstrates there are no periodic solutions or other time-dependent attractors therein. Based on its invariant property, the following argument shows there are no periodic solutions *anywhere* in the phase space. The projection of a three-dimensional periodic solution on the (x, y)-plane must also be periodic (it may of course cross itself) and any such projection must lie completely on one side or the other of the line $x = y$ since no solutions cross the quarterplane $x = y$. However, the derivative pair $(\mathrm{d}x/\mathrm{d}t, \mathrm{d}y/\mathrm{d}t)$ can only assume the signs $(+, +)$, $(-, +)$, and $(-, -)$, on, say, the $y > x$ region (see figure 3*c*), and it is therefore impossible to have a periodic projection and hence any periodic solutions. This argument extends to *any* time-dependent solution that after some interval returns arbitrarily close to itself. In particular, there are no quasi-periodic or almost-periodic solutions. The three steady-state pure modes are the only asymptotically stable convection patterns. They are competing attractors in phase space, and their domains of attraction partition the space into three regions separated by separatrix surfaces or sheets (figure 5).

Part of the system of separatrix surfaces can be determined without computing. Indeed, by symmetry part of the $x = y$ quarterplane must separate the domains of attraction for the x-roll and y-roll. Another surface separates the domains of the three-dimensional pattern from the roll cells. It must pass through the separatrix curves in the $x = y$, $x = 0$, and $y = 0$ quarterplanes. However, these separatrix curves must be obtained numerically.

One of the most accurate ways to locate this bounding surface is by its intersection with another surface which meets it roughly perpendicularly. It is convenient to use a plane $x + y + z =$ constant in phase space as the intersecting surface. Then the relative areas of the surface regions on this 'energy' shell give the probabilities of

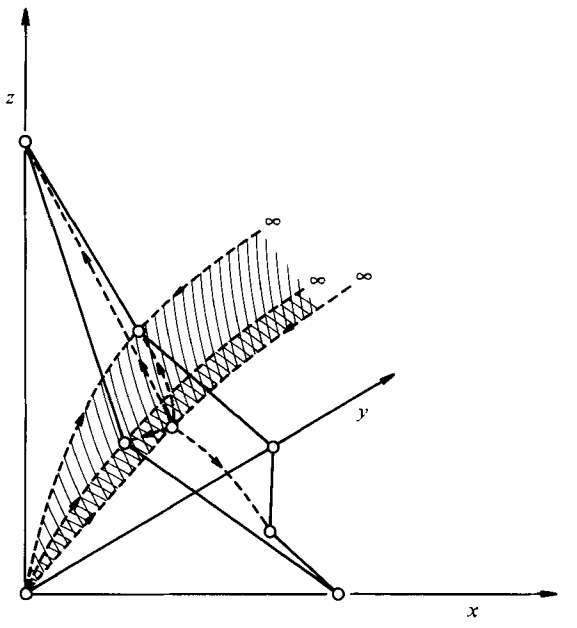

FIGURE 5. The phase space for the cubic box and $R/R_c > 1.218$, showing the surface which separates the region of disturbances attracted by the three-dimensional convection pattern (pure mode z) from those attracted by one of the roll cells (pure mode x or y). The solutions (circles) are connected with each other and the point at infinity by separatrix curves (dashed) which form boundaries for the separating surface. The solid lines connect the convection solutions, which lie on the faces of the octant and relate the structure to that shown in figure 3(*c*).

pattern selection for a disturbance with that norm or 'energy'. Of course, since the solutions are those of a nonlinear system, the relative areas will vary with the particular constant of the shell. Furthermore, to generate the probability for equally likely disturbances of amplitude less than a certain value, a sequence of such energy-shell calculations can be made and the results appropriately weighted and summed.

We illustrate these ideas with a shell calculation for the cubic box at $R = 50$ which is just above the point of stabilization of the three-dimensional mode. We admit disturbances with unit norm

$$x+y+z = 1,$$

which corresponds to the set of points represented by an equilateral triangle through $(1,0,0)$, $(0,1,0)$ and $(0,0,1)$ in the positive octant. In general, the boundaries of the domains of attraction within this triangle must be mapped out numerically. Each of the four endpoints of these bounding curves lies on the separatrix curve in one of the four invariant quarterplanes. We calculate the endpoints first. On the $z = 0$ face, symmetry forces the endpoint to be $(\frac{1}{2}, \frac{1}{2}, 0)$ (see figure 6). For the others, by starting a trajectory near enough the mixed 2-mode (a saddle point) and reversing the sense of time so that trajectories are exponentially attracted to the separatrix connected with infinity, accurate approximations of the point where the separatrix crosses the energy shell can be achieved numerically. In order to fill in the curves shown in figure 6, initial conditions are chosen close to that unique stable trajectory of the mixed 2-mode which originates at the mixed 3-mode (the reversal in time direction is maintained). The accuracy of the boundaries of figure 6 depends only on the accuracy

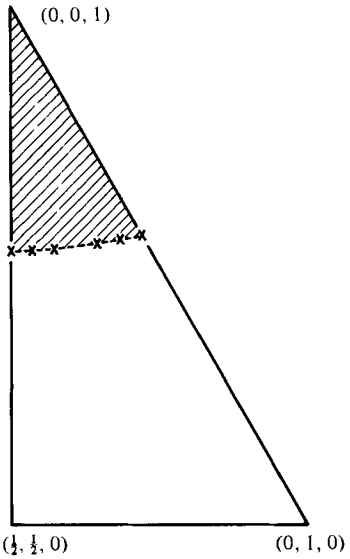

FIGURE 6. A triangular slice through phase space showing its intersection with the domain of attraction of the three-dimensional pattern (shaded) for the cubic box at $R = 50$. The 'separatrix' surface (figure 5) intersects this triangle in a curve which is estimated numerically by observing where trajectories pierce it (× marks).

of the numerical approximation. The shaded area represents the domain of attraction for the three-dimensional mode and constitutes 21 % ± 2 % of the total area. Therefore, provided all disturbances of unit norm are equally likely, there is a 21 % chance that the three-dimensional convection pattern will be selected at $R = 50$. As R increases from 50, plane III moves relative to planes I and II (figure 3*c*) in such a way that this probability increases to some limiting value. Of course, if certain disturbances are more likely than others, a distribution of weights can be assigned to the points in phase space.

5.4. *Comparison with previous results*

We first specialize our results for the cubic box to the case examined by Zebib & Kassoy (1978): the x- and y-rolls are the only primary modes. These interact to produce one secondary mode [112], which in turn mixes with the primaries to reproduce a primary. The resulting amplitude equations are recovered from system (5.5) by putting $z \equiv 0$, evaluating the coefficients at $(h_1, h_2) = (1, 1)$, and approximating R by R_c in the nonlinear terms. Taking account of Zebib & Kassoy's different scaling of their governing system puts the resulting amplitude equations in a form identical with their system (Zebib & Kassoy 1978, equations (15)), obtained by a standard perturbation method.

In their analysis of the amplitude equations, Zebib & Kassoy point out that, in addition to the finite-amplitude x- and y-roll convection states, there is another solution, a prescribed linear combination of those rolls, which we call the (x, y) mixed 2-mode. They calculated that this nominally three-dimensional convection state transfers less heat near critical than the roll patterns but did not compute its stability. Our analysis (§5.2) demonstrates that it is unstable at least up to $R = 60$. Furthermore, our results show those amplitude equations are accurate only for $R \leqslant 4.5\pi^2$, at which point the [111]-mode is unstable by linear theory and becomes a finite-amplitude

convection state. However, since this new finite-amplitude pattern remains unstable, the truncation with two primary modes continues to give *qualitatively* correct information concerning the stable finite-amplitude patterns up to $R = 4.87\pi^2$. Thereafter, though, say at $R = 50$, we see that more than one in five random disturbances of unit norm will go to *neither* x- nor y-roll; the qualitative picture has changed significantly.

Straus & Schubert (1979, 1981) have studied the finite-amplitude convection patterns that occur in porous media by using a numerical scheme based on Galerkin's method. They have focused on the cubic geometry (1979) and boxes with square planform (1981).

Among others (Holst & Aziz 1972; Horne 1978), they have pointed out that different disturbances may lead to distinct stable steady convection patterns; in particular, over a broad range of Rayleigh number ($R < 150$), both two-dimensional patterns dominated by a roll-cell and a three-dimensional pattern dominated by the [111]-mode can be achieved. The lowest Rayleigh number for which such competition is reported is $R = 60$, well above the value $R = 48.06$ where we predict the three-dimensional [111]-mode is first observable.

Although they leave for later study the question of why certain random disturbances go to one pattern rather than another, it is noted that emphasis of a particular mode in the initial condition can force a particular convection pattern. This is understood for $R < 60$ in terms of our phase-space picture and its domains of attraction (figure 5). This picture shows exactly which contributions to the initial conditions will lead to the three-dimensional pattern. Furthermore, our probability calculation supplies a characterization of how random disturbances will evolve.

The heat-transfer characteristics across the box are expressed by the Nusselt number

$$N \equiv 1 - h_1 h_2 \int\int_A \left|\frac{\partial \theta}{\partial z}\right| \mathrm{d}x\,\mathrm{d}y, \tag{5.9}$$

which when evaluated at the two- and three-dimensional convection patterns given in §5.2 yields respectively

$$N_{2\mathrm{D}} = 1 - 2\pi a_{002,\,2\mathrm{D}} = 1 + 4\left(1 - \left[\frac{R_{101}}{R}\right]^{\frac{1}{2}}\right), \tag{5.10}$$

$$N_{3\mathrm{D}} = 1 - 2\pi a_{002,\,3\mathrm{D}} = 1 + \frac{\pi A^2}{8E}\left(1 - \left[\frac{R_{111}}{R}\right]^{\frac{1}{2}}\right), \tag{5.11}$$

where R_{111}, R_{101}, A and E are defined as functions of (h_1, h_2) and R by (3.2) and (5.6a, e) respectively. Equations (5.10) and (5.11) apply for those $R < 60$ where the solutions exist and for (h_1, h_2) near $(2^{\frac{1}{2}}, 2^{\frac{1}{2}})$. Straus & Schubert (1979) report the heat transferred by the three-dimensional pattern in the cube from its birth ($4.5\pi^2 \leqslant R$), even though it is unstable up to $R = 4.87\pi^2$. Up to about $R = 55$, (5.11) gives values which cannot be distinguished from the numerical results (which are accurate to within 1 %). The agreement is still good at $R = 60$, where (5.11) predicts 5 % too-little heat transfer. As R increases further, the agreement continues to deteriorate on the low side. This occurs since the amplitude of a_{111} has become sufficiently large that in conjunction with sufficiently numerous interaction paths a sum of $O(a_{111}^4)$ contributions affects the heat transfer. Indeed, the [113]-mode, produced by the $\boldsymbol{N}(\boldsymbol{x}_{111}, \boldsymbol{x}_{022})$, $\boldsymbol{N}(\boldsymbol{x}_{111}, \boldsymbol{x}_{202})$ and $\boldsymbol{N}(\boldsymbol{x}_{111}, \boldsymbol{x}_{002})$ interactions, becomes large enough to affect the heat transfer through its contribution (upon remixing with [111]) to the [002] and [004] temperature

fields. This indicates that, for a better approximation, higher-order interaction paths and more modes must be accounted for.

Over the interval from convection onset to $R = 60$ the two-dimensional rolls transfer more heat than the three-dimensional solution, since for fixed Rayleigh number they are farther from their point of instability given by linear theory, and hence of larger amplitude. The situation changes at higher Rayleigh numbers where higher-order interactions boost the amplitude of the three-dimensional solution at a faster rate than the roll cells, eventually eliminating the 'headstart' of the latter. At $R = 60$, $N_{2D} \approx 1.11 N_{3D}$, and Straus & Schubert find that the curves cross at $R \approx 97$.

The two-dimensional Nusselt dependence given by (5.10) for the cube is within 1 % of the corresponding numerical results of Straus & Schubert (1979) for $R_c \leqslant R \leqslant 60$. In light of the above discussion this may at first seem contradictory since if higher-order effects become significant for the three-dimensional pattern they certainly must be more significant for the roll cell, which has a larger amplitude for these Rayleigh numbers. However, it is the *combination* of amplitude and number of interaction paths which determines the total effect and in this case the roll cell has $\frac{1}{3}$ the interaction paths available. Indeed, the nonlinearity eliminates two of three paths which are accessible to the three-dimensional pattern since

$$\langle \boldsymbol{x}_{202}, \boldsymbol{N}(\boldsymbol{x}_{101}, \boldsymbol{x}_{101}) \rangle = \langle \boldsymbol{x}_{022}, \boldsymbol{N}(\boldsymbol{x}_{101}, \boldsymbol{x}_{101}) \rangle = 0. \tag{5.12}$$

Neither the [202]- nor [022]-mode is produced in the self-interaction of the roll cell. A calculation using relative pattern amplitudes at $R = 60$ shows that this inaccessibility can reduce the sum of 4th-order effects from 4 % to 1 % of total, which corresponds roughly to the deviations we note between the predictions of (5.11) and (5.10) and the 'exact' solutions respectively.

Special cases of (5.10) have been reported previously. Zebib & Kassoy (1978) give the heat transferred by a roll cell in a cube based on the same interactions that yield (5.10). Using a different technique, the 'power-integral' approach, Combarnous & Bories (1975) compute the transfer by roll cells across a horizontally infinite layer. They find the same form (for $R < 60$) as Zebib & Kassoy:

$$N_{2D} = 1 + 2\left(1 - \frac{R_c}{R}\right). \tag{5.13}$$

Equations (5.10) and (5.13) have identical asymptotic behaviours for small $(R - R_c)/R_c$, as we expect. However, as this parameter grows they deviate, until, at $R = 60$, (5.13) gives a value 4 % below (5.10) and the 'exact' numerical solution. Hence, the approximation (5.10) seems to converge to the exact solution over a broader range of Rayleigh numbers. Finally, we note that (5.10) also agrees with the expansion of Palm, Weber & Kvernvold (1972) over this range of Rayleigh numbers.

Provided that the roll cell fits within the lateral boundaries, a requirement that affects the critical value R_{101}, the nonlinear heat transfer is not otherwise influenced by its container, since the only intermediary in the interaction, the motionless temperature field, fits all containers. On the other hand, the three-dimensional pattern is influenced by the mediating [202]- and [022]-modes, whose amplitude is moderated by lateral walls. For tall thin boxes of approximately square planform ($A \to \infty$), the effect of these modes becomes negligible, since little heat is transferred via them. However, the critical value R_{111} will be strongly influenced by such a geometry change.

In qualitative terms, our results for $R < 60$ support and model many of the features

observed in numerical studies over a much broader range of Rayleigh number (Straus & Schubert 1979; Horne 1978). Furthermore, our Nusselt-number results show excellent *quantitative* agreement up to $R = 60$, supporting the claim that our truncation accurately represents the behaviour up to that point.

5.5. *The stretched box*

We now consider a box for which the y-dimension is stretched by 20% from the cube $(h_1, h_2) = (1, 1.2)$. Convection onset occurs at $R_c = 39.48$ where the x-roll goes unstable by linear theory (figure 2). Soon after, at $R = 40.81$, the y-roll goes unstable, followed by the [111]-mode at $R = 42.29$. Linear theory also tells us that the [021]-mode, the most unstable of those not included in the sum (5.1), is neutrally stable at $R = 50.71$. This is an *a priori* upper limit in Rayleigh number to the accuracy of the approximation.

By an analysis like that described in detail for the cubic box, we obtain the existence and stability changes for the finite-amplitude states as Rayleigh number increases from convection onset. These may be summarized in the bifurcation diagrams (figure 7), an alternative to the birth chart. The amplitudes of the components of the steady solution are plotted as a function of distances from convection onset. The pure modes are labelled by 'p' and the components of the mixed mode by the type of mixture. For example, the branches labelled (x, z) in the a_{101} and a_{111} pictures give the amplitudes of the corresponding eigenfunctions whose linear combination constitutes an (x, z) mixed 2-mode solution. All the branches are symmetric about zero amplitude, and several distinct convection patterns can be constructed from a single mixed-mode solution by switching the signs of the constituent amplitudes.

The points of linear instability mark the births of the pure modes. The stability of these and existence and stability of the other solutions are determined by nonlinear effects. Instability (local) is represented by dashed curves in figure 7. The x-roll is stable from birth to the limit of Rayleigh numbers of interest. As the y-roll and three-dimensional pattern come into existence, they are unstable to the x-roll owing to its strength. The x-roll remains the sole stable pattern until $R = 44.65$, when an (x, z) mixed mode is born (unstable) and the finite-amplitude [111]-pattern simultaneously stabilizes. At this point the amplitude a_{111} has become large enough to overcome the attraction to the x-roll exerted through the (x, z) nonlinear interaction. This growth in amplitude to sufficient size is the result of two effects. First the [111]-mode is sufficiently far from its point of linear instability, and secondly the [111]–[111]-mode resonant nonlinear interaction (represented in part by $|\boldsymbol{N}(\boldsymbol{x}_{111}, \boldsymbol{x}_{111})|$) is weak enough to permit the growth. At $R = 46.86$ the y-roll undergoes a similar stability change, yielding three stable convection patterns. The (x, y) mixed 2-mode, which comes into being at that point, is unstable, as is the (y, z) 2-mode that was produced earlier ($R = 43.45$). Finally, at $R = 54.83$ (beyond the expected interval for accurate approximation), the mixed 3-mode is born and is unstable. In this Rayleigh-number regime other modes which have become linearly unstable may begin to play a significant role in the interaction. Furthermore, when the amplitudes are large enough, higher-order interactions will be important regardless of the stability status (by linear theory) of the modes involved.

For the stretched box the stable convection patterns give a Nusselt number proportional to the square of the amplitudes. Over the interval of Rayleigh number under consideration, this gives the x-roll transferring more heat than the y-roll, which

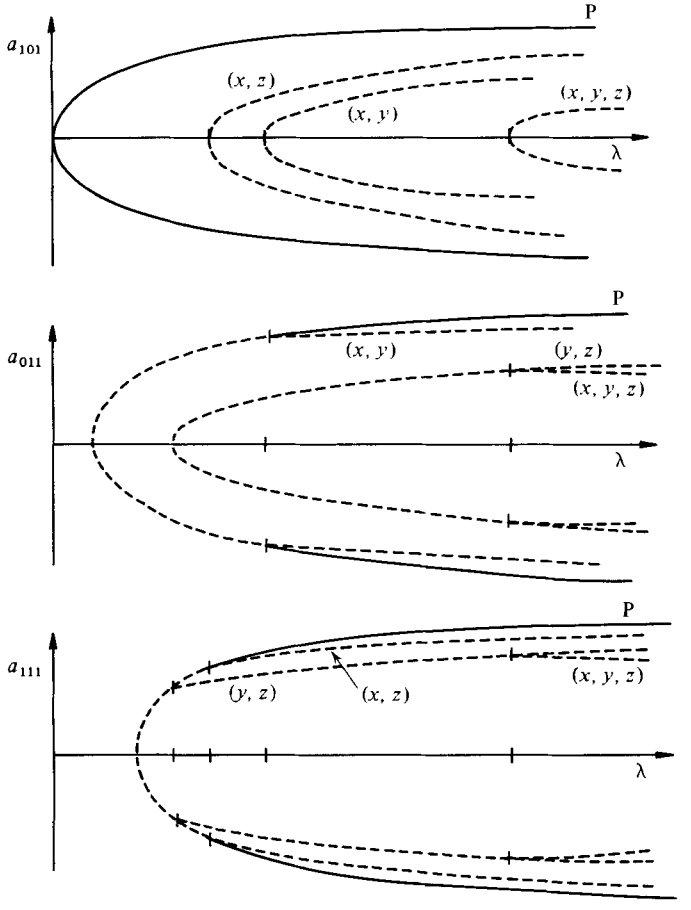

FIGURE 7. The bifurcation diagram for a box with dimensions 1:1.2:1 gives the constituent amplitudes as a function of distance λ from convection onset. The pure modes P are stable (solid line) over certain segments, and the mixed modes, labelled by their constituents, are all everywhere unstable.

in turn transfers more heat than the three-dimensional pattern. With increasing Rayleigh number, the gap between these curves decreases.

We note that all the bifurcations represented in figure 7 are of supercritical type (they open to the right) and that the only stable modes are pure modes. Furthermore, once they stabilize, these pure modes remain stable (within the context of the particular truncation). This is characteristic of supercritical bifurcations at single eigenvalues, and hence the qualitative behaviour of the stable solutions might have been guessed from a simpler nonlinear analysis. However, results from other geometries show that this need not be the case.

6. Summary

We consider convection in cubic and nearly cubic boxes of porous material and obtain the full set of steady convection patterns for Rayleigh numbers $1 \leqslant R/R_c < 1.5$. For these geometries three of the linear modes go unstable at Rayleigh numbers near one another, and using a 'splitting' parameter the convective states are analysed as

bifurcations near a multiple eigenvalue. Up to $R/R_c \approx 1.5$, the interactions between the unstable modes dominate the behaviour, which is captured by considering nonlinear effects to third order. For $R/R_c \approx 1.5$, fourth-order interactions become large enough to contribute 5% to the heat transport, and new modes not accounted for begin to grow according to linear theory; the approximation breaks down there.

When the conduction solution goes unstable in the cubic box at $R = 39.48$ x- and y-roll finite-amplitude patterns grow with Rayleigh number and compete within phase space to attract disturbances. At $R = 48.06$ a finite-amplitude three-dimensional pattern becomes stable and joins the competition. As R increases, its domain of attraction expands, taking territory from the x- and y-roll patterns; at $R = 50$ we predict a 21% chance that a disturbance with certain fixed norm will go to the three-dimensional pattern. Over the range of Rayleigh numbers considered, the birth (existence) of a finite-amplitude pattern with structure corresponding to a mode of linear theory coincides with the linear instability of that mode. The finite-amplitude stability, however, depends upon the linear growth rate of the mode (distance from point of linear instability) as well as nonlinear interactions with the other modes. Indeed, immediately above convection onset, the x- and y-rolls have larger amplitudes than the third existing convection pattern, and the rolls are stable. When the three-dimensional pattern comes into existence the rolls continue to dominate until that pattern gains sufficient amplitude to overcome the attractions caused by nonlinear interactions. Only then does it gain stability. Such existence and stability results can be read off a simple geometric construction in phase space.

The nonlinear system of ordinary differential equations that governs the modal interactions has coefficients which we calculate as explicit functions of the aspect ratios and Rayleigh number. This permits an analysis of boxes with non-square planform, in addition to providing an explicit dependence of heat-transport properties on geometry. For example, stretching the y-dimension of the box by 20% increases the heat transferred by the three-dimensional pattern by 6% at $R = 50$. Such a geometry change also modifies the existence and stability results; these are described in detail.

The results of Zebib & Kassoy (1978) are recovered as a subcase of our calculations for the cubic box. We show that the cross-roll pattern they discover is unstable and remains so (at least up to $R = 60$), and we obtain the limits in Rayleigh number at which their analysis ceases to give a good approximation.

Furthermore, the sequence of existence and stability events for $R_c \leqslant R < 60$ corrects several details reported by Straus & Schubert (1981). In particular, the superposition of orthogonal two-dimensional rolls, or the cross-roll, is not an observed motion. Also, the symmetric [111]-dominated steady solution gains stability ($R = 48.06$) somewhat after it comes into existence ($R = 44.41$).

The phase-space pictures we obtain for the locally stable competing convection patterns gives complete information about how each pattern can lose stability to another. These pictures provide insight into what has been observed over a broad range of Rayleigh number in previous numerical computations.

The author is indebted to Professor G. M. Homsy for (i) the suggestion that convection in a box near the triple eigenvalue could be fruitfully analysed using Rosenblat's method – the idea on which this paper is based – and (ii) his generous support throughout this project.

The author would also like to thank Professor S. Rosenblat for several useful

discussions and Dr Alan Jepson for his advice concerning the numerical computation of separatrix surfaces.

This work was done at Stanford University under partial support of the Office of Basic Sciences of the U.S. Department of Energy.

REFERENCES

BAUER, L., KELLER, H. & REISS, E. 1975 *SIAM Rev.* **17**, 101.

BECK, J. L. 1972 *Phys. Fluids* **15**, 1377.

COMBARNOUS, M. A. & BORIES, S. A. 1975 *Adv. Hydrosci.* **10**, 231.

ECKHAUS, W. 1965 *Studies in Nonlinear Stability Theory*. Springer.

ELDER, J. W. 1967 *J. Fluid Mech.* **27**, 29.

HARTMAN, P. H. 1964 *Ordinary Differential Equations*. Wiley.

HOLST, P. H. & AZIZ, K. 1972 *Intl J. Heat Mass Transfer* **15**, 73.

HOMSY, G. M. & SHERWOOD, A. E. 1976 *AIChE J.* **22**, 168.

HORNE, R. N. 1979 *J. Fluid Mech.* **92**, 751.

MARCUS, P. S. 1981 *J. Fluid Mech.* **103**, 241.

PALM, E., WEBER, J. E. & KVERNVOLD, O. 1972 *J. Fluid Mech.* **54**, 153.

ROSENBLAT, S. 1979 *Stud. Appl. Maths* **60**, 241.

ROSENBLAT, S. 1982 *J. Fluid Mech.* **122**, 395.

ROSENBLAT, S., DAVIS, S. H. & HOMSY, G. M. 1982 *J. Fluid Mech.* **120**, 91.

SCHNEIDER, K. J. 1963 In *Proc. Intl Congr. Refrig., 11th, Munich*, Paper 11–4.

STRAUS, J. M. & SCHUBERT, G. 1979 *J. Fluid Mech.* **91**, 155.

STRAUS, J. M. & SCHUBERT, G. 1981 *J. Fluid Mech.* **103**, 23.

TREVE, Y. M. & MANLEY, O. P. 1982 *Physica* **D4**, 319.

ZEBIB, A. & KASSOY, D. R. 1978 *Phys. Fluids* **21**, 1.